Journal of Extracellular Vesicles

RESEARCH ARTICLE OPEN ACCESS

GCC2 in Small Extracellular Vesicles as a Diagnostic and Prognostic Biomarker of Early-Stage Lung Adenocarcinoma

Byeong Hyeon Choi[1,2,3] | Hyonggin An[4] | Sukki Cho[5,6] | Sungsoo Lee[7] | Hyeong Ryul Kim[8] | Jong Ho Cho[9] | Jun Hee Lee[1,2] | Ga Yoon Kim[1,2] | Ok Hwa Jeon[1,2] | Hyunku Shin[10] | Yeonho Choi[10,11] | Hyun Koo Kim[1,2,3]

[1]Department of Thoracic and Cardiovascular Surgery, Korea University Guro Hospital College of Medicine, Korea University, Seoul, Republic of Korea | [2]Image Guided Precision Cancer Surgery Institute, Korea University, Seoul, Republic of Korea | [3]Department of Biomedical Sciences, College of Medicine, Korea University, Seoul, Republic of Korea | [4]Department of Biostatistics, Korea University College of Medicine, Seoul, Republic of Korea | [5]Department of Thoracic and Cardiovascular Surgery, Seoul National University College of Medicine, Seoul, Republic of Korea | [6]Department of Thoracic and Cardiovascular Surgery, Seoul National University Bundang Hospital, Seongnam-si, Gyeonggi-do, Republic of Korea | [7]Department of Thoracic and Cardiovascular Surgery, Gangnam Severance Hospital, Yonsei University College of Medicine, Seoul, Republic of Korea | [8]Department of Thoracic and Cardiovascular Surgery, Asan Medical Center, University of Ulsan College of Medicine, Seoul, Republic of Korea | [9]Department of Thoracic and Cardiovascular Surgery, Samsung Medical Center, Sungkyunkwan University School of Medicine, Seoul, Republic of Korea | [10]EXoPERT Corporation, Seoul, Republic of Korea | [11]Department of Biomedical Engineering, Korea University, Seoul, Republic of Korea

Correspondence: Yeonho Choi (yeonhochoi@korea.ac.kr) | Hyun Koo Kim (kimhyunkoo@korea.ac.kr)

Received: 19 June 2025 | **Revised:** 30 January 2026 | **Accepted:** 2 March 2026

Keywords: lung adenocarcinoma | diagnosis | prognosis | liquid biopsy | small extracellular vesicles | GCC2

ABSTRACT

Emerging evidence suggests that GRIP and coiled-coil domain-containing two enriched small extracellular vesicles (sEV-GCC2) may serve as diagnostic biomarkers of early-stage lung adenocarcinomas. However, the roles of these molecules remain unclear. This study evaluated the diagnostic and prognostic potential of sEV-GCC2 for detecting early-stage lung adenocarcinoma and its tumourigenic role *in vitro* and *in vivo*. This retrospective multicentre study analyzed 470 plasma samples (320 lung adenocarcinoma patients, 150 controls; mean follow-up: 34.7 ± 24.0 months) across five institutions. Size-exclusion chromatography and enzyme-linked immunosorbent assay were used to measure sEV-GCC2 levels, whereas immunohistochemistry was used to confirm GCC2 expression in tumour tissues. Functional studies were performed using the PC9 and H1650 lung adenocarcinoma cell lines in vitro and the corresponding PC9-based preclinical models in vivo to evaluate the tumour-related effects of sEV-GCC2. Patients exhibited significantly elevated sEV-GCC2 levels compared to controls (area under the receiver operating characteristic (ROC) curve [AUC]: 0.904, $P < 0.001$), with similar results in stage TisN0–T1miN0 disease (AUC: 0.781, $P < 0.001$). sEV-GCC2 levels were associated with the pathological TNM stage and tumour location. Higher sEV-GCC2 levels were correlated with poorer recurrence-free survival (RFS), overall survival and recurrence rates, even in patients with stage 0–IA1 disease. Functional studies have revealed that sEV-GCC2, but not GCC2-deficient sEVs, promote cancer cell proliferation, tumour growth and lymph node

Abbreviations: ADC, adenocarcinoma; ARRIVE, animals in research: reporting in vivo experiments; ApoB, apolipoprotein B; AUC, area under the curve; CD63, cluster of differentiation 63; CI, confidence interval; CPM, counts per million; CT, computed tomography; EEA1, early endosome antigen 1; EGFR, epidermal growth factor receptor; ELISA, enzyme-linked immunosorbent assay; ESCRT, endosomal sorting complexes required for transport; FBS, fetal bovine serum; GAPDH, glyceraldehyde 3-phosphate dehydrogenase; GCC2, golgi coiled-coil protein 2; GM130, golgi matrix protein 130; HRP, horseradish peroxidase; IHC, immunohistochemistry; KD, knockdown; miRNA, microRNA; NSCLC, non-small cell lung cancer; NPV, negative predictive value; NTA, nanoparticle tracking analysis; OS, overall survival; PBS, phosphate-buffered saline; PCR, polymerase chain reaction; PPV, positive predictive value; RFS, recurrence-free survival; ROC, receiver operating characteristic; RR, recurrence rate; RPMI, roswell park memorial institute; STAT4, signal transducer and activator of transcription 4; STARD, standards for the reporting of diagnostic accuracy studies; STING, stimulator of interferon genes; sEV, small extracellular vesicle; sEV-GCC2, small extracellular vesicles enriched with GRIP and coiled-coil domain-containing 2; siRNA, small interfering RNA; TMM, trimmed mean of M-values; TNM, tumour-node-metastasis.

Byeong Hyeon Choi and Hyonggin An have contributed equally to this work and share first authorship

metastasis *in vitro* and *in vivo*. These findings highlight the diagnostic and prognostic potential of sEV-GCC2 and its tumourigenic role in early-stage lung adenocarcinoma. This study was registered at ClinicalTrials.gov (NCT04529915)

1 | Introduction

Lung cancer is the leading cause of cancer-related deaths worldwide. Non-small cell lung cancer (NSCLC) accounts for 85% of all lung cancer cases (Siegel et al. 2025). NSCLC can be classified into several subtypes, including adenocarcinoma (ADC), squamous cell carcinoma and large cell carcinoma (Travis et al. 2015). Lung ADC accounts for the majority of primary lung cancer cases and is associated with a high incidence and poor prognosis (Russell et al. 2011). The 5-year overall survival rate for lung ADC is stage-dependent, ranging from 92% for stage IA1 to < 1% for stage IVB disease, despite advances in medical technology (AmericanCancerSociety 2018; Goldstraw et al. 2016). Thus, novel strategies that facilitate the early and accurate diagnosis of lung ADC are needed to reduce mortality rates, prolong survival and improve the prognosis and quality of life of patients.

Clinical guidelines in most countries recommend annual screening for the detection of lung cancer (Mazzone et al. 2018). Lung cancer is diagnosed based on the results of imaging examinations such as low-dose computed tomography (CT) (Mulshine and Sullivan 2005; Reck and Rabe 2017). Conventional diagnostic examinations are expensive, involve radiation exposure, and exhibit low sensitivity for early identification of cancerous lesions (Mazzone et al. 2021). Owing to their invasive nature, repeated low-dose CT scans and bronchoscopy-guided biopsies are not recommended for histopathological diagnosis. Therefore, low-risk and convenient screening methods for early diagnosis of lung cancer are warranted.

Current approaches to lung cancer treatment include surgical and pharmaceutical interventions, and treatment choice depends on prognostic factors (Bott et al. 2015). However, predicting the prognosis of patients who have not undergone surgery or in whom clear prognostic information cannot be obtained from surgical tissue examinations is particularly challenging (Adachi et al. 2017; Birim et al. 2005). Various methods, such as CT, positron emission tomography/CT, biopsies (bronchoscopy or CT-guided) and surgical pathological staging (Birim et al. 2005), have been used to determine the stage of lung cancer, which is crucial for predicting prognostic outcomes. Surgical pathological staging, the most accurate and reliable method for predicting cancer prognosis, involves evaluating resected specimens and lymph nodes. This method is associated with the risk of bleeding, which may hinder lymph node dissection. The nodal status may be underestimated in patients undergoing non-anatomical resection (Robinson et al. 2020). Thus, new prognostic tools that offer more precise and personalized treatment strategies are required, even for challenging cases.

Liquid biopsy is superior to other methods for predicting the diagnosis and prognosis of patients with cancer, owing to its non-invasive, repeatable and highly sensitive nature (Pantel and Alix-Panabières 2019; Rolfo et al. 2018). However, conventional cancer biomarkers have shown inadequate diagnostic and prognostic accuracy (Hoseok and Cho 2015). There is an unmet need for promising biomarkers with high diagnostic and prognostic accuracy for early-stage lung cancer detection.

Small extracellular vesicles (sEVs), defined as vesicles with a diameter of 30–200 nm that are secreted by all cell types, are involved in various biological functions, such as tumourigenesis, drug resistance, angiogenesis, metastasis and cell-to-cell communication (Xu et al. 2018). sEVs carry the molecular identities of their parental cells, such as DNA, miRNAs and proteins, and have emerged as promising disease biomarkers (Jayaseelan 2020). However, the utility of sEVs as biomarkers for lung cancer remains unclear, and their use is yet to be approved by the Food and Drug Administration (Bardelli and Pantel 2017; Palmirotta et al. 2018).

In a pilot study using a limited patient cohort, our team identified GRIP and coiled-coil domain-containing 2 (GCC2)-enriched small extracellular vesicles (sEV-GCC2) as potential diagnostic biomarkers for early lung adenocarcinoma (ADC) (Jeong et al. 2021). However, the clinical and biological significance of sEV-GCC2 has not yet been validated in a large pathologically confirmed population, and its prognostic relevance and functional involvement in lung ADC progression remain unclear (Jeltema et al. 2023; Tu et al. 2022).

Recent studies have reported the overexpression of GCC2-linked molecules, including ALK fusion genes and the antisense RNA GCC2-AS1, in lung ADC, which are associated with drug resistance, metastasis, poor survival and tumourigenesis (Jiang et al. 2018; Vendrell et al. 2017; F. Yu et al. 2021a).

To address these issues, the present multicentre study validated the diagnostic and prognostic utility of sEV-GCC2 in early-stage lung ADC using a large cohort and investigated its tumour-promoting role through complementary in vitro and in vivo analyses.

2 | Methods

2.1 | Ethical Approval

This multicentre, retrospective clinical study was approved by the Institutional Review Board of Korea University Guro Hospital (2020GR0176) and by the institutional IRBs of all participating institutions (ClinicalTrials.gov ID: NCT04529915). This study was conducted in accordance with the principles of the Declaration of Helsinki. The preclinical animal experiments were approved by the Institutional Animal Care and Use Committee of Korea University (KOREA-0216-0223-C1).

This study adhered to the Standards for the Reporting of Diagnostic Accuracy Studies (STARD) and Reporting

Recommendations for Tumor Marker Prognostic Studies (REMARK) guidelines (Bossuyt et al. 2015; Kilkenny et al. 2012; Sauerbrei et al. 2018) (Supplemental files 1 and 2). All animal experiments were conducted according to the ARRIVE (Animals Research: Reporting In Vivo Experiments) guidelines (see Supplemental File 3) (Kilkenny et al. 2012).

2.2 | Human Participants and Blood Collection

Blood plasma samples and clinical data were obtained from patients treated at five hospitals in the Republic of Korea: Korea University Guro Hospital, Seoul National University Bundang Hospital, Yonsei University Gangnam Severance Hospital, Asan Medical Center and Samsung Medical Center. Plasma samples were collected retrospectively, and clinical data were collected prospectively.

The inclusion criteria were as follows: (1) Korean adults; (2) patients who underwent surgical resection for pathologically confirmed stage Tis, T1mi, T1a–T1c, or T2a–T2b lung cancer; (3) stage N0 or N1 disease; (4) no history of chemotherapy or radiotherapy before surgery; and (5) no previous diagnosis of cancer prior to lung cancer surgery. Patients who did not meet these criteria were excluded.

Baseline data included age, sex, smoking history, histological subtype, primary tumour location, pathological TNM (pTNM) stage, invasion pattern, EGFR mutation type, tumour size, pathological upstaging and recurrence or survival status.

Plasma samples from patients with lung ADC were collected intraoperatively between February 2013 and September 2020 and stored in biobanks at the five participating centres. Control plasma samples were obtained from healthy individuals without a history of cancer and were provided by the Biobank of Seoul National University Bundang Hospital. All plasma samples were processed via centrifugation and stored at –80°C without freeze-thaw cycles.

2.3 | Isolation of sEVs From Blood Plasma and Cell Culture Medium

An Exo-i size-exclusion chromatography-based sEV isolation kit (EXoPERT Inc., Seoul, Republic of Korea) was used in accordance with the manufacturer's instructions to isolate sEVs from 500 μL of blood plasma. Plasma samples were collected from each participating centre and processed using the same kit under identical experimental conditions following a standardized protocol in a single laboratory with technical support from the kit manufacturer.

The cells were cultured to 70–80% confluence, rinsed twice with phosphate-buffered saline (PBS; Cat. #10010-023; Thermo Fisher Scientific), and cultured in Roswell Park Memorial Institute (RPMI) 1640 medium (Gibco, Waltham, MA, USA) to isolate sEVs. The conditioned medium was collected and centrifuged at 500 × *g* for 10 min at 4°C after 48 h of incubation. The cellular debris was removed by centrifugation at 5,000 × *g* for 30 min at 4°C. An Amicon Ultra-15 centrifugal filter (100 KDa; Cat. #UFC910024; Merck Millipore) was used to collect and concentrate the supernatant according to the manufacturer's instructions. An Exo-i size-exclusion chromatography-based sEV isolation kit (EXoPERT Inc.) was used following the manufacturer's instructions to purify a 500-μL aliquot of the concentrated supernatant.

2.4 | Nanoparticle Tracking Analysis

A NanoSight NS300 instrument (Malvern Instruments Ltd., Worcestershire, UK) was used to analyze the size distribution and concentration of sEVs. Each experiment was performed in triplicate. A NanoSight Nanoparticle Tracking Analyzer (NTA) 2.3 analytical software (Malvern Instruments Ltd.) was used for data analysis.

2.5 | Transmission Electron Microscopy

Purified sEVs were placed on 300-mesh Formvar carbon-coated copper grids (cat. No. FCF300 - Cu - 50; Electron Microscopy Science, Hatfield, PA, USA) for 10 min. A solution of 1% phosphotungstic acid (in phosphate buffer) was prepared, and a drop of the staining solution was added to the copper mesh with the sample using a dropper. The staining solution was subsequently removed using a filter paper, and the grid was air-dried for 10 min. A transmission electron microscope (H7650; Hitachi, Tokyo, Japan) was used to obtain the images at 120 kV.

2.6 | Western Blotting

The purified sEVs were incubated with protein lysis buffer, and a Bradford assay was performed to determine the protein concentration. Proteins were separated by 8 or 12% sodium dodecyl sulfate-polyacrylamide gel electrophoresis and horizontally transferred onto nitrocellulose membranes. Membranes were incubated with primary antibodies obtained from Santa Cruz Biotech, Dallas, TX, USA: CD63 (SC-15363), TSG101 (SC-7964), ApoB (SC-13538), calnexin (SC-23954), GM130 (SC-55591), GCC2 (No. A13814, Abclonal, Boston, MA, USA) and EEA1 (No. 14-9114-8214, Invitrogen, Carlsbad, CA, USA). The membrane was subsequently incubated with m-IgGk BP-HRP (SC-516102) or mouse anti-rabbit IgG-HRP (SC-2357) as secondary antibodies.

Enhanced chemiluminescence reagent (DoGenBio Co., Seoul, Republic of Korea) was used to visualize the protein bands. Densitometry was performed using ImageJ 1.8.0 (National Institutes of Health, Bethesda, MD, USA) to determine relative protein expression, normalized to the control group.

2.7 | GCC2 Enzyme-Linked Immunosorbent Assay

A GCC2 enzyme-linked immunosorbent assay kit (MyBioSource, San Diego, CA, USA) was used to quantify GCC2 expression according to the manufacturer's instructions. In brief, 50 μL of plasma-derived sEVs and 100 μL of HRP-conjugated reagent were added to each well of the plate, covered with a membrane plate sealer, and incubated at 37°C for two hours. A 1:1 mixture of chromogen solutions A and B was added to each well after washing the wells four times with the wash solution, and the plate was incubated in the dark at 37°C for 15 min. The reaction was

terminated by adding 50 μL of stop solution. A SpectraMax 190 Microplate Reader (Molecular Devices Corp., San Jose, CA, USA) was used to measure the absorbance at 450 nm.

2.8 | Hematoxylin & Eosin Staining

All samples were deparaffinised in xylene. A graded series of aqueous ethanol solutions (100, 90, 80 and 70%) was used for gradual rehydration. The samples were stained with hematoxylin, differentiated in 1% hydrochloric acid, rinsed with tap water until the nuclei became blue, and counterstained with eosin for two minutes. The samples were dehydrated in a series of ethanol solutions (twice in 90% ethanol for 5 s each, and twice in 100% ethanol for 5 min each) and cleared in xylene (twice for < 1 min each). Samples were rinsed twice with 70% ethanol, purified twice with xylene, and mounted in an aqueous solution (Cat. #AML060; ScyTek Laboratories Inc., Logan, UT, USA). The prepared samples were observed under a microscope.

2.9 | Immunohistochemistry Staining

Formalin-fixed paraffin-embedded lung tissue sections, 4-μm thick, were subjected to immunohistochemistry (IHC) analysis using the following standard protocols. The sections were deparaffinized in xylene, rehydrated using a graded series of ethanol solutions, and incubated in 3% H_2O_2 at room temperature for 15 min. The slides were incubated overnight at 4°C with GCC2 antibodies following heat-mediated retrieval. Secondary antibody staining with 3,3′-diaminobenzidine was performed using the Polink-2 Plus HRP Broad Kit (GBI Labs, Bothell, WA, USA). An automatic bioimage analysis software (SABIA Version 3.0; EBIOGEN Inc., Seoul, Republic of Korea) was used to perform quantitative IHC analysis.

2.10 | Cell Culture

PC9 and H1650 (human lung adenocarcinoma) cells were cultured in RPMI 1640 medium (Gibco, Grand Island, NY, USA) supplemented with 10% fetal bovine serum (FBS; Gibco, Grand Island, NY, USA) and 1% penicillin–streptomycin (Gibco, Grand Island, NY, USA) in 5% CO_2 at 37°C. sEVs in FBS were depleted by ultracentrifugation at 180,000 × g (T-647.5, fixed-angle rotor, Sorvall WX 100 Plus, Thermo Fisher Scientific, IN, USA) at 4°C for 18 h to obtain sEVs free of FBS.

2.11 | Small Interfering RNA Transfection

PC9 and H1650 cells were transfected with small interfering RNAs (siRNAs) targeting GCC2 (Accell Human GCC2 siRNA; Cat. #E-013457-00-00010, Dharmacon Inc., Lafayette, CO, USA), or control siRNA (Accell non-targeting control siRNA, Cat. #D-001910-01-05, Dharmacon Inc.) according to the manufacturer's instructions for the knockdown of GCC2 mRNA and protein expression.

PC9 and H1650 cells were seeded at 1×10^5 cells per dish in 60-mm cell culture dishes and cultured in 5 mL of RPMI 1640 for 24 h or until cells reached 60–80% confluence. The cells were transfected with the corresponding siRNAs at a final concentration of 1 nmol according to the manufacturer's instructions. The siRNA-containing serum-free cell delivery medium (Horizon, NJ, USA) was replaced with the RPMI 1640 medium after 72 h.

2.12 | Quantitative Real-Time Polymerase Chain Reaction

Total RNA, extracted from cells using TRIzol reagent (Invitrogen, Carlsbad, CA, USA) and chloroform, was precipitated using isopropanol. AccuPower RT PreMix (Bioneer, Daejeon, Republic of Korea) was used to synthesize complementary DNA with the following primers:

GCC2 F: 5′-AAACCTCTGCGGAACAGCACCA-3′ and R: 5′-GAACTCGGACTTTGTAGCTCTCG-3′; GAPDH F: 5′-ATCATCCCTGCCTCTACTGG-3′ and R: 5′-CCCTCCGACGCCTGCTTCAC-3. ' The QuantStudio 6 Flex Real-Time PCR System (Thermo Fisher Scientific) with SYBR Green PCR Master Mix (Cat. #4367659; AB Science, Paris, France) was used to perform qRT-PCR in triplicate.

2.13 | Wound Healing Assay

PC9 and H1650 cells were seeded in 12-well plates at 3×10^5 cells/well and cultured in 5% CO_2 at 37°C for at least 24 h to facilitate cell adhesion and the formation of a confluent monolayer. The confluent monolayer was scratched with a 1 mL sterile pipette tip. PBS or 100 μg of exosomes was subsequently added to the culture medium. All scratch assays were performed in triplicate. An IX71-F32PH inverted microscope (Olympus) was used to capture images at each time point. ImageJ 1.50i (https://imagej.nih.gov/ij/) was used to analyze three fields per well.

2.14 | Cell Proliferation Assay

PC9 cells were seeded at a density of 5×10^3 cells/well in 96-well plates (in triplicate) and treated with exosomes (total, 10, 50 and 100 μg/well) for 24, 48 and 72 h. Subsequently, 50 μL of 0.5 mg/mL 3-(4,5-dimethylthiazol-2-yl)-2,5-diphenyltetrazolium bromide (MTT; cat. #M5655; Sigma-Aldrich Inc.) was added to the cells at the end of each time point, and the plates were incubated for two hours at room temperature. The culture supernatant was removed, and 150 μL of dimethyl sulfoxide was added to the cells to solubilize the MTT precipitates. A SpectraMax 96-plate reader was used to measure optical density at 460 nm.

2.15 | Mouse Xenograft Cancer Model

Five-week-old female BALB/c nude mice were purchased from Orient Bio (Gyeonggi-do, Republic of Korea), bred and housed under specific-pathogen-free conditions. For tumour establishment, 1×10^6 PC9 or PC9-GCC2 KD cells were injected into the footpad of each mouse. After excluding mice without tumours, mice with successfully established tumours were divided into PC9, PC9-GCC2 knockdown (PC9-GCC2 KD), PC9-GCC2 KD with sEV-GCC2 and PC9-GCC2 KD with sEV-GCC2 KD groups ($n = 4$ for each group). The mice in each group were housed in individual cages with free access to food and water to facilitate acclimatization.

The mice in the PC9 group received a subcutaneous injection of 1×10^6 PC9 control cells in the footpad; those in the PC9-GCC2 knockdown (PC9-GCC2 KD) group received 1×10^6 GCC2-knockdown PC9 cells (20 μL); those in the PC9-GCC2 KD with sEV-GCC2 group received PC9-GCC2 KD cells and 100 μg of sEV-GCC2 (20 μL); and those in the PC9-GCC2 KD with sEV-GCC2 KD group received 1×10^6 PC9 cells and 100 μg of GCC2-knockdown sEVs (20 μL).

Calipers were used to measure the tumour size on alternate days. The tumour volume was calculated using the following standard formula:

$$V = L \times W \times H/2$$

where L, W and H represent the length, width and height of the tumour, respectively. The popliteal lymph nodes were harvested after euthanasia. To assess lymph node metastasis, harvested popliteal lymph nodes were evaluated histopathologically. H&E staining was performed to evaluate metastatic involvement, and GCC2 IHC was performed on serial sections.

The metastatic burden was assessed by (i) the proportion of mice with lymph node metastases, (ii) semi-quantitative grading of metastatic burden per lymph node and (iii) quantification of the GCC2-positive area within the lymph nodes. All histological evaluations were performed using identical criteria across the experimental groups.

2.16 | Small RNA Sequencing of sEVs

Small RNA sequencing was performed using sEVs isolated from conditioned media of PC9 wild-type cells and GCC2-knockdown PC9 cells ($n = 3$ biological replicates per group). Total RNA was extracted from sEVs, and the quality was assessed using an Agilent 2100 Bioanalyzer. Small RNA libraries were constructed using the NEBNext Low-Bias Small RNA Library Prep Kit according to the manufacturer's instructions. Sequencing was performed on an Illumina NextSeq 2000 platform with single-end 75 bp reads.

Raw sequencing reads were subjected to quality control and adapter trimming using Trim Galore (trim_galore v0.6.6), which integrates Cutadapt. Processed reads were aligned to the human reference genome (hg38), and microRNA was annotated based on miRbase v22. Read counts were normalized using the trimmed mean of M-values (TMM) and counts per million (CPM) methods implemented in edgeR. All sequencing and bioinformatic analyses were conducted by e-Biogen (Seoul, Republic of Korea).

2.17 | Statistical Analysis

All statistical analyses were performed using IBM SPSS Statistics (version 22.0; IBM Corp., Armonk, NY, USA), MedCalc version 20.023 (MedCalc Software, Mariakerke, Belgium) and GraphPad Prism (version 9.0; GraphPad Software, San Diego, CA, USA).

Categorical variables were compared using the chi-square test or Fisher's exact test, and continuous variables were analyzed using the independent sample *t*-test or Mann-Whitney U test, as appropriate. Spearman's rank correlation evaluated non-parametric associations between variables.

Receiver operating characteristic (ROC) curve analysis assessed the diagnostic performance of sEV-GCC2, total sEV concentration, and sEV size. ROC analyses comparing patients with healthy controls were adjusted for age and sex. The areas under the ROC curves (AUCs) were compared using the DeLong test when applicable.

Multivariate logistic regression analysis examined the association between sEV-GCC2 levels and lung adenocarcinoma after adjusting for pTNM stage, tumour location in the left lower lobe, tumour size and visceral pleural invasion. Variables included in the multivariate models were selected based on their clinical relevance and univariate significance ($P < 0.1$).

Cutoff values for survival analyses were determined using the Youden index (J = sensitivity + specificity − 1), as thresholds based on the mean, median or quartiles of sEV-GCC2 did not yield statistically significant stratification.

Survival outcomes were analyzed using Kaplan–Meier curves with log-rank tests and Cox proportional-hazards regression. False discovery rate correction was applied to *P* values from survival analyses. Events were defined as recurrence (RR), overall survival (OS; death from any cause) and recurrence-free survival (RFS; time to recurrence or death). Time-to-event was calculated from the date of surgery to the occurrence of the event.

Box-and-whisker plots were used to visualize the data distributions, showing the median and interquartile range (25th–75th percentiles). Statistical significance was set at $P < 0.05$.

3 | RESULTS

3.1 | Plasma sEV Characterization

In total, 470 blood plasma samples obtained from 150 controls and 320 patients with lung ADC were analyzed in this study. The overall study flow is summarized in Table S1. Among the 320 lung ADC samples, 100, 70, 50, 50 and 50 were obtained from Korea University Guro Hospital, Seoul National University Bundang Hospital, Yonsei University Gangnam Severance Hospital, Asan Medical Center and Samsung Medical Center, respectively. Table 1 summarizes the clinical characteristics of participants.

Nanoparticle tracking analysis (NTA), transmission electron microscopy (TEM) and western blotting were performed to validate the quality and identity of sEVs isolated from blood plasma (Figure 1). TEM revealed cup- or dish-shaped vesicles with diameters ranging from 30 to 200 nm (Figure 1A). Western blot analysis demonstrated strong expression of canonical sEV markers (CD63 and TSG101) and the absence of non-sEV markers (ApoB, calnexin) (Figure 1B).

NTA revealed a significantly higher concentration of sEVs in patients with lung ADC than in healthy controls (approximately

TABLE 1 | Characteristics of the study participants.

		Controls (%)	Patients with lung ADC (%)	*P*-value
Sex	**Male**	78 (52.0)	144 (45.0)	< 0.0001
	Female	72 (48.0)	176 (55.0)	
Age, years (mean ± SD)		57.0 ± 4.5	65.8 ± 9.0	< 0.0001
Smoking history	**Non-smoker**	85 (56.7)	205 (64.1)	0.486
	Smoker	21 (14.0)	34 (10.6)	
	Ex-smoker	44 (29.3)	81 (25.3)	
Histology	**Adenocarcinoma**	—	320	—
Site of tumour	**Right upper lobe**	—	85 (26.6)	—
	Right middle lobe		32 (10)	
	Right lower lobe		67 (20.9)	
	Left upper lobe		80 (25)	
	Left lower lobe		56 (17.5)	
pTNM stage	**TisN0**	—	5 (1.6)	—
	T1miN0		16 (5)	
	T1aN0		31 (9.7)	
	T1bN0		73 (22.8)	
	T1cN0		68 (21.3)	
	T2aN0		88 (27.5)	
	T2bN0		22 (6.9)	
	T1cN1		4 (1.3)	
	T2aN1		10 (3.1)	
	T2bN1		3 (0.9)	
Invasion type	**Visceral pleural**	—	76 (23.8)	—
	Lymphatic		55 (17.2)	
	Venous		25 (7.8)	
	Lymphatic with venous		42 (13.1)	
	Lymphatic with visceral- pleural		24 (7.5)	
	None		98 (30.6)	
EGFR type	**Wild**	—	76 (23.75)	—
	Mutation		124 (38.75)	
	Not tested		120 (37.50)	
Tumour size (mm)	**Mean ± SD**	—	24.7 ± 1.8	—
Follow up duration (months)	**Mean ± SD**	—	34.7 ± 24.0	

ADC, adenocarcinoma; pTNM stage, pathological TNM stage; SD, standard deviation.

1.37-fold increase; $P < 0.0001$), with no significant difference in vesicle size (Figures 1C and D).

3.2 | Elevated sEV-GCC2 Levels in Lung Adenocarcinoma

The plasma concentration of sEV-GCC2 was significantly elevated in patients with lung adenocarcinoma (ADC) compared to that in healthy controls (66.4 vs. 40.3 pg/mL; 1.6-fold increase; $P < 0.0001$; Figure 2A). A stage-wise increase in sEV-GCC2 levels was also observed, with significantly higher concentrations in stage IB-IIB tumours than in stage 0-IA3 tumours ($P < 0.0001$; Figure 2B).

ROC analysis demonstrated that sEV-GCC2 had the highest diagnostic performance among all sEV-based indicators, yielding an AUC of 0.904 (95% CI: 0.876–0.932), sensitivity of 83.75%, specificity of 88.0%, positive predictive value (PPV) of 93.7% and negative predictive value (NPV) of 71.7% (Figure 2C; Table S2).

In the TisN0–T1miN0 subgroup, sEV-GCC2 levels were significantly elevated compared to those in the healthy controls ($P < 0.0001$; Figure 2D). The corresponding age- and sex-adjusted ROC curve analysis showed an AUC of 0.781 (95% CI: 0.690–0.861) with a sensitivity of 71.43%, specificity of 94.67%, PPV of 65.2% and NPV of 95.9% (Figure 2E).

Comprehensive substage analysis further validated this upward trend, demonstrating that sEV-GCC2 levels were significantly elevated across all lung ADC subgroups, from TisN0–T1miN0 to

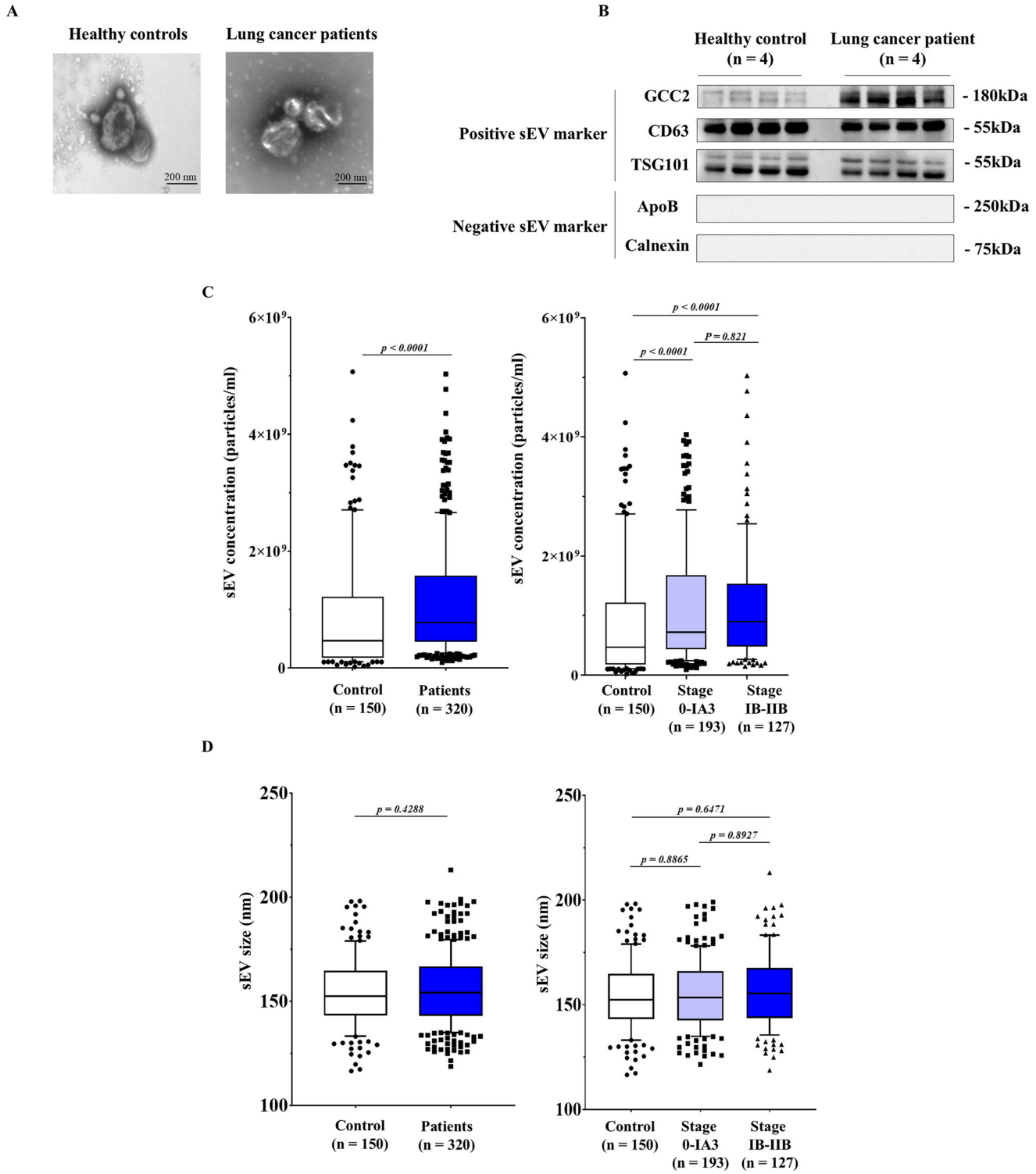

FIGURE 1 | **Characterization of small extracellular vesicles (sEVs) isolated from human plasma**. (A) Transmission electron microscopy (TEM) images of sEVs isolated from the plasma of healthy individuals and patients with lung adenocarcinoma (ADC), showing characteristic vesicular morphology. (B) Western blot analysis of sEV-associated markers (CD63, TSG101), non-sEV markers (ApoB, calnexin) and GCC2 in sEVs from controls and ADC patients. (C) Nanoparticle tracking analysis (NTA) of sEV concentration in both groups. (D) NTA of sEV size distribution. Scale bar = 200 nm.

stage IIB, compared to controls ($P < 0.0001$ for all comparisons; Figure 3). These findings highlight the utility of sEV-GCC2 as a sensitive biomarker spanning the full spectrum of early-stage lung ADC, from pre-invasive lesions to more advanced pathological stages.

Multivariate regression analysis showed that the sEV-GCC2 concentration was independently associated with pathological TNM stage ($P = 0.001$) and tumour location in the left lower lobe ($P = 0.010$) (Table 2), reinforcing its clinical utility as a non-invasive biomarker for early-stage lung ADC.

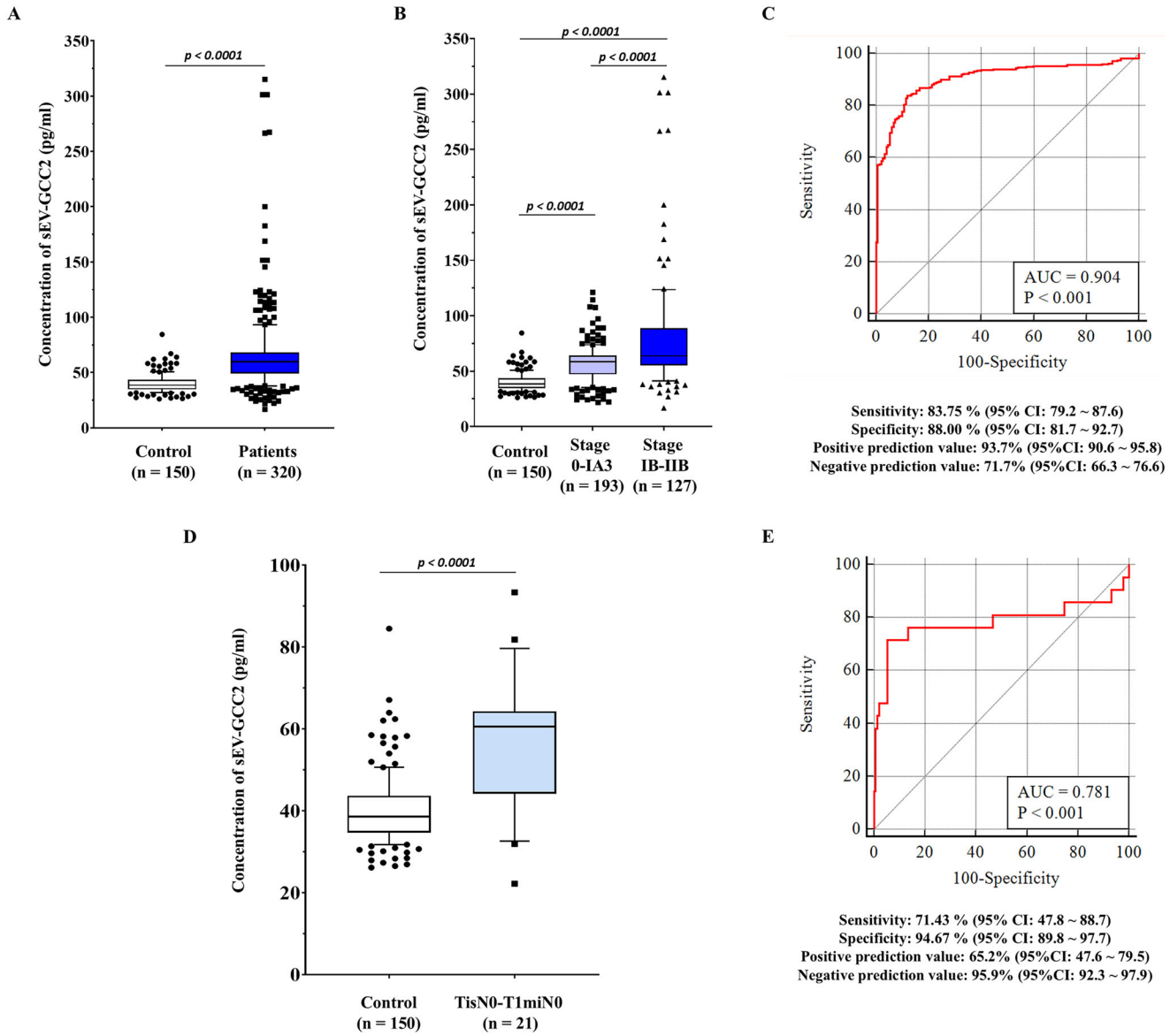

FIGURE 2 | Plasma sEV-GCC2 concentrations across pathological stages of lung adenocarcinoma (ADC) and corresponding diagnostic performance. (A) Comparison of sEV-GCC2 concentrations between healthy controls ($n = 150$) and all patients with lung ADC ($n = 320$). (B) sEV-GCC2 concentrations stratified by pathological stage: stage 0-IA3 (n = 193) and stage IB-IIB (n = 127). (C) ROC analysis evaluating the diagnostic performance of sEV-GCC2 in distinguishing all lung ADC patients from healthy controls, with adjustment for age and sex. (D) Comparison of sEV-GCC2 concentrations between healthy controls and patients with carcinoma in situ or minimally invasive disease (TisN0–T1miN0, $n = 21$). (E) ROC analysis for sEV-GCC2 in the TisN0–T1miN0 subgroup versus healthy controls, adjusted for age and sex.

In a supplementary analysis, sEV-GCC2 concentrations stratified by lung lobe location are shown in Figure S1.

3.3 | Tumour GCC2 Overexpression and Plasma sEV-GCC2 Levels Predict Pathological Up-staging

Immunohistochemical analysis demonstrated that GCC2 expression was markedly elevated in lung ADC tissues compared to that in adjacent normal tissues, with an 8.9-fold increase ($P < 0.0001$; Figures 4A-C). GCC2 levels were significantly higher in stage II tumours than in stage I tumours ($P < 0.0001$; Figure 4D). These findings support the hypothesis that tumour-derived GCC2 contributes to the elevated plasma levels of sEV-GCC2 observed in patients with lung ADC.

Building on this observation, we examined whether sEV-GCC2 levels in the preoperative plasma could reflect pathological disease progression. Among the 320 patients with lung ADC, 148 experienced pathological upstaging after surgery, whereas 172 did not; of the latter, 117 showed no change in stage and 55 were downstaged (Table S3). Down staging results are not presented because they were not significant. Patients in the up-staging group had significantly higher preoperative sEV-GCC2 concentrations than those in the no-change group ($P = 0.0221$; Figure 5). ROC curve analysis revealed that sEV-GCC2 yielded a modest but significant predictive value for pathological up-

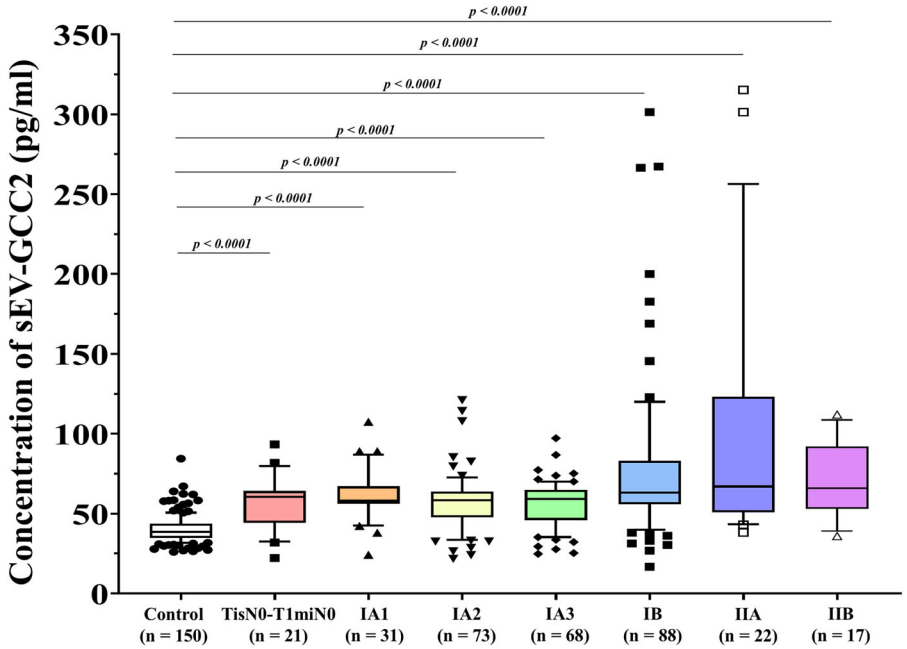

FIGURE 3 | Distribution of plasma sEV-GCC2 concentrations by pathological TNM stage in patients with lung adenocarcinoma. Box-and-whisker plots display sEV-GCC2 concentrations across pathological TNM substages.

TABLE 2 | Univariable and multivariable analysis of sEV-GCC2 with factors in lung adenocarcinoma patients.

Variable		Univariable			Multivariable		
		β	95%CI	*P*-value	*β*	95%CI	*P*-value
Age		−0.008	−0.453 to 0.393	0.890			
Sex		−0.012	−9.188 to 7.329	0.825			
Body surface area		−6.151	−24.793 to 123.491	0.517			
Smoking history		−0.039	−6.449 to 3.074	0.486			
pTNM stage		0.309	15.591 to 31.609	< 0.0001	0.291	8.938 to 35.528	0.001
Tumour location	**RLL**	−0.008	−10.873 to 9.325	0.880			
	RUL	−0.045	−13.078 to 5.510	0.424			
	RML	0.070	−5.018 to 22.309	0.214			
	LUL	−0.079	−15.756 to 2.591	0.159			
	LLL	0.143	3.274 to 24.680	0.011	0.136	3.218 to 23.463	0.010
Tumour size		0.282	6.036 to 13.270	< 0.0001	0.123	−0.386 to 8.803	0.072
Lymphatics invasion		0.038	−7.100 to 14.667	0.494			
Visceral pleura invasion		0.126	1.415 to 20.573	0.025	−0.084	−19.889 to 5.262	0.253
Venous invasion		−0.009	−16.498 to 14.122	0.879			
EGFR mutation		0.009	−7.700 to 9.143	0.866			
sEV concentration		0.048	-1.8×10^9 to 4.7×10^9	0.393			
sEV particle size		0.018	−0.200 to 0.280	0.745			

Abbreviations: LLL, left lower lobe; LUL, left upper lobe; pTNM, pathological TNM; RLL, right lower lobe; RML, right middle lobe; RUL, right upper lobe.

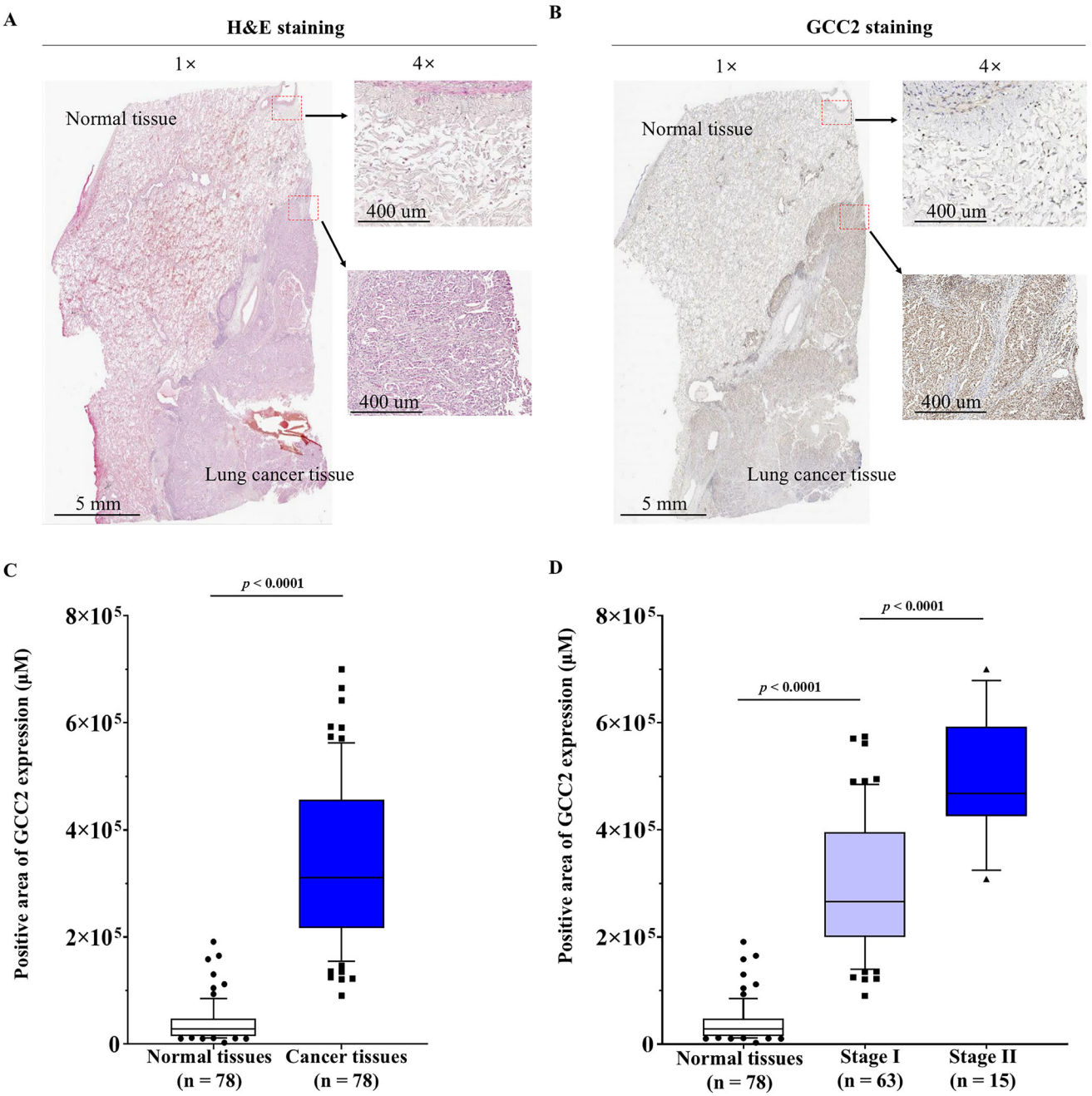

FIGURE 4 | Histological and immunohistochemical analysis of GCC2 expression in lung adenocarcinoma tissues. (A) Hematoxylin and eosin staining of representative lung adenocarcinoma tissue sections showing normal and tumour regions at 1× magnification with corresponding 4× magnification views of the indicated areas. (B) Immunohistochemical staining for GCC2 in representative lung adenocarcinoma tissue sections is shown at 1× magnification with corresponding 4× magnification views of the indicated regions. (C) Quantitative comparison of GCC2 expression between normal lung tissue ($n = 78$) and lung adenocarcinoma tissue ($n = 78$). (D) GCC2 expression levels stratified by pathological stage (normal tissues vs stage I vs. stage II). Scale bars: 5 mm (1×) and 400 μm (4×).

staging (AUC = 0.582; 95% CI: 0.520–0.642; $P = 0.024$; Figure 5).

These findings suggest that elevated plasma sEV-GCC2 levels may serve not only as a diagnostic marker but also as a potential indicator of subclinical tumour aggressiveness, thereby aiding postoperative therapeutic decision-making in early-stage lung ADC.

3.4 | High sEV-GCC2 Predicts Poor Prognosis after Surgical Resection of Lung ADC

A cut-off value of 73.88 pg/mL for sEV-GCC2 was determined using the Youden index and applied to stratify patients for survival analysis. Kaplan–Meier analysis revealed that patients with high sEV-GCC2 levels (≥ 73.88 pg/mL) had significantly worse RR and RFS after surgery compared to those with lower

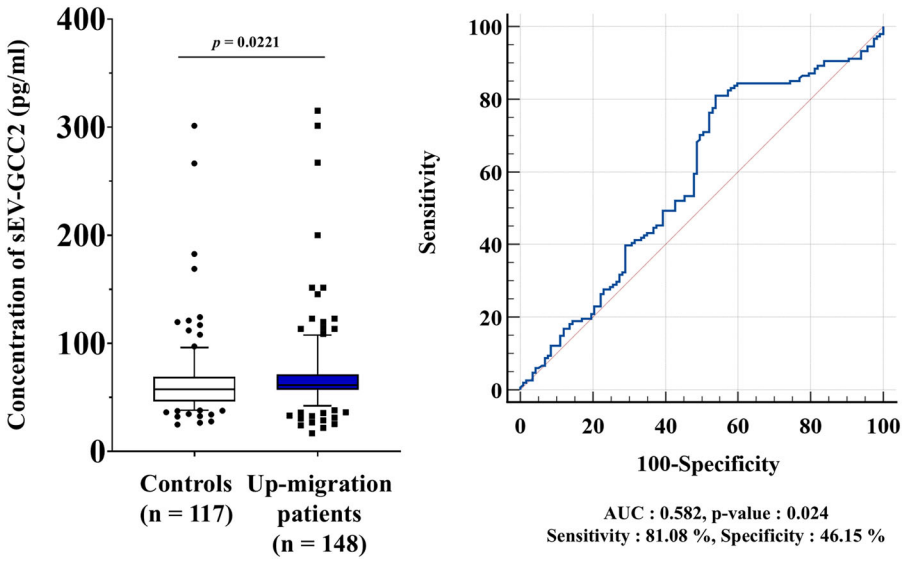

FIGURE 5 | **Plasma sEV-GCC2 levels predict pathological up-staging in patients with lung adenocarcinoma**. Receiver operating characteristic (ROC) curve analysis comparing sEV-GCC2 concentrations between patients without pathological stage change (no-change group, $n = 117$) and those with pathological up-staging after surgery ($n = 148$).

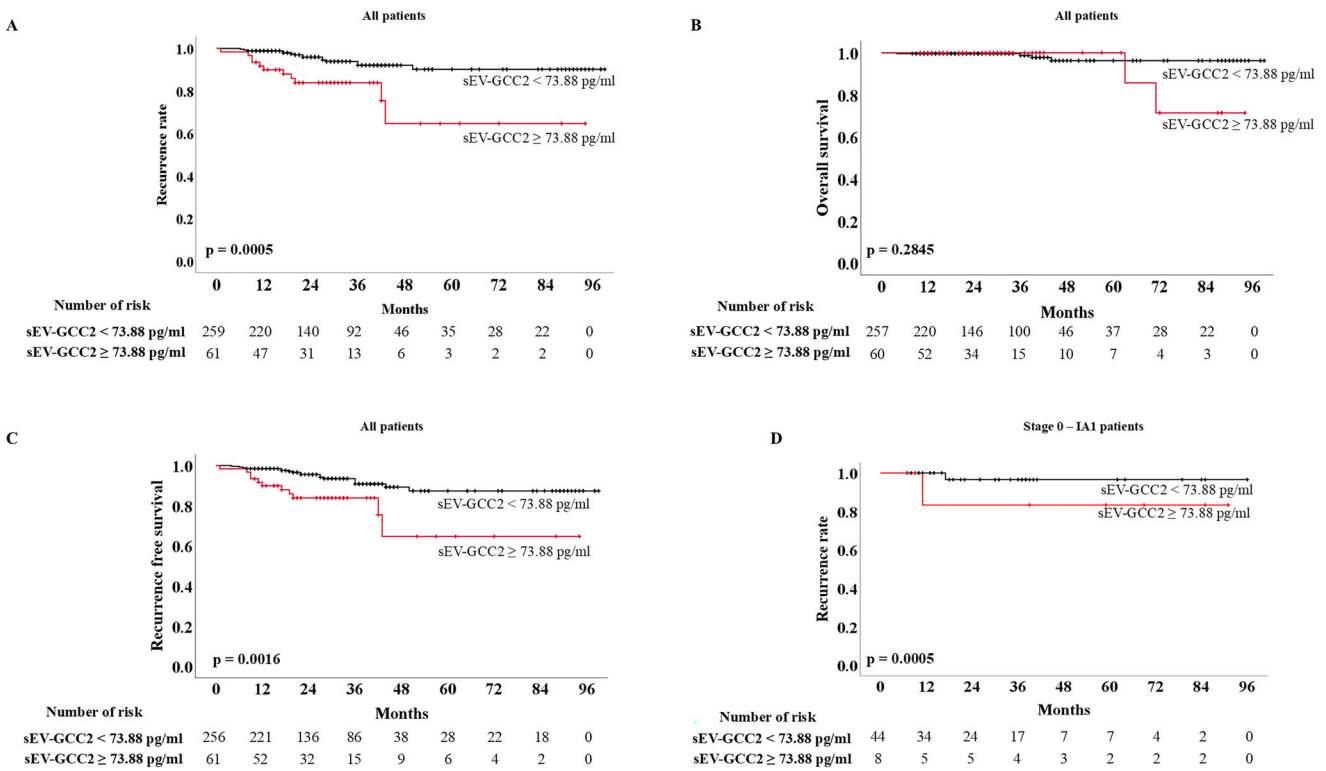

FIGURE 6 | Kaplan–Meier analysis of time to recurrence, overall survival, and recurrence-free survival. (A) Recurrence rates and sEV-GCC2 concentrations in all patients. (B) Analysis of overall survival and sEV-GCC2 concentrations in all patients. (C) Recurrence-free survival rates and sEV-GCC2 concentrations in all patients. (D) Recurrence rate and sEV-GCC2 concentrations in patients with stages 0–IA1 disease. False discovery rate correction was applied for survival analyses, and adjusted p-values are shown.

levels. Specifically, the median time to recurrence was 77.7 months in the high sEV-GCC2 group versus 93.3 months in the low group ($P = 0.0005$; Figure 6A), and the median RFS was 71.0 months versus 90.3 months, respectively ($P = 0.0016$; Figure 6C). Although OS showed a downward trend in the high sEV-GCC2 group, this difference was not statistically significant ($P = 0.2845$; Figure 6B).

In the stage 0–IA1 subgroup, high sEV-GCC2 levels were still significantly associated with worse recurrence ($P = 0.0005$; Figure 6D), although no deaths were recorded in this cohort. Similar trends were observed in stage-specific analyses; patients with stage IA3 and IB disease showed significantly poorer RR and RFS when sEV-GCC2 levels were elevated ($P = 0.001$ for both; Figure S2 and S3). In patients with stage IIB disease, high sEV-GCC2 levels were associated with significantly higher recurrence rates ($P = 0.0083$; Figure S4).

Cox proportional hazards analysis revealed that RR was independently associated with tumour location in the left lower lobe ($P = 0.041$), pathological N stage ($P = 0.002$), lymphatic invasion ($P = 0.014$) and sEV-GCC2 concentration ($P = 0.004$) (Table 3). RFS demonstrated similar associations with these variables, including sEV-GCC2 concentration (RFS: $P = 0.018$).

These findings indicate that elevated preoperative sEV-GCC2 levels are independently associated with unfavourable clinical outcomes after curative-intent surgery. Collectively, these results highlight the prognostic utility of sEV-GCC2 as a non-invasive biomarker that reflects tumour biology and enables risk stratification for recurrence and survival in early-stage lung ADC.

3.5 | Functional Validation of GCC2 and sEV-GCC2 in Lung Adenocarcinoma Progression

To explore the functional role of GCC2 in lung ADC progression, PC9 and H1650 cell lines were engineered using targeted siRNAs to stably suppress GCC2 expression (Figure S5A and B). In vitro wound healing assays demonstrated that GCC2 knockdown markedly impaired cell migration at 24 and 72 h compared to control cells in both cell lines ($P < 0.0001$), suggesting that GCC2 facilitates motility in lung cancer cells (Figure S5C).

Next, we assessed whether GCC2 contained in sEVs contributed to tumour aggressiveness. sEVs were isolated from the conditioned media of PC9 and GCC2-deficient PC9 cells (Figures 7A and B). GCC2 knockdown effectively reduced the GCC2 content within secreted sEVs, while classical sEV markers (CD63 and TSG101) remained detectable, and the Golgi marker GM130 was absent.

Consistent with this observation, immunoblot analysis revealed that cellular depletion of GCC2 was accompanied by reduced expression of the early endosomal marker EEA1 and the ESCRT-I component TSG101 in both PC9 and H1650 cells, whereas Alix expression was relatively preserved (Figure S6), suggesting impaired sEV biogenesis upon GCC2 knockdown.

Functionally, sEVs containing GCC2 significantly promoted the proliferation of GCC2-deficient PC9 cells in a dose-dependent manner, whereas sEVs from GCC2-silenced cells suppressed cell growth (Figure 7C). In vivo, footpad injection of GCC2-deficient PC9 cells along with sEV-GCC2 led to a ~6.7-fold increase in tumour volume compared to injection with sEV-GCC2-depleted vesicles ($P < 0.0001$; Figure 7D). The animals treated with sEV-GCC2 exhibited more frequent and extensive lymph node metastases than those treated with GCC2-depleted sEVs (Figure 7E). Consistent with these histological observa-

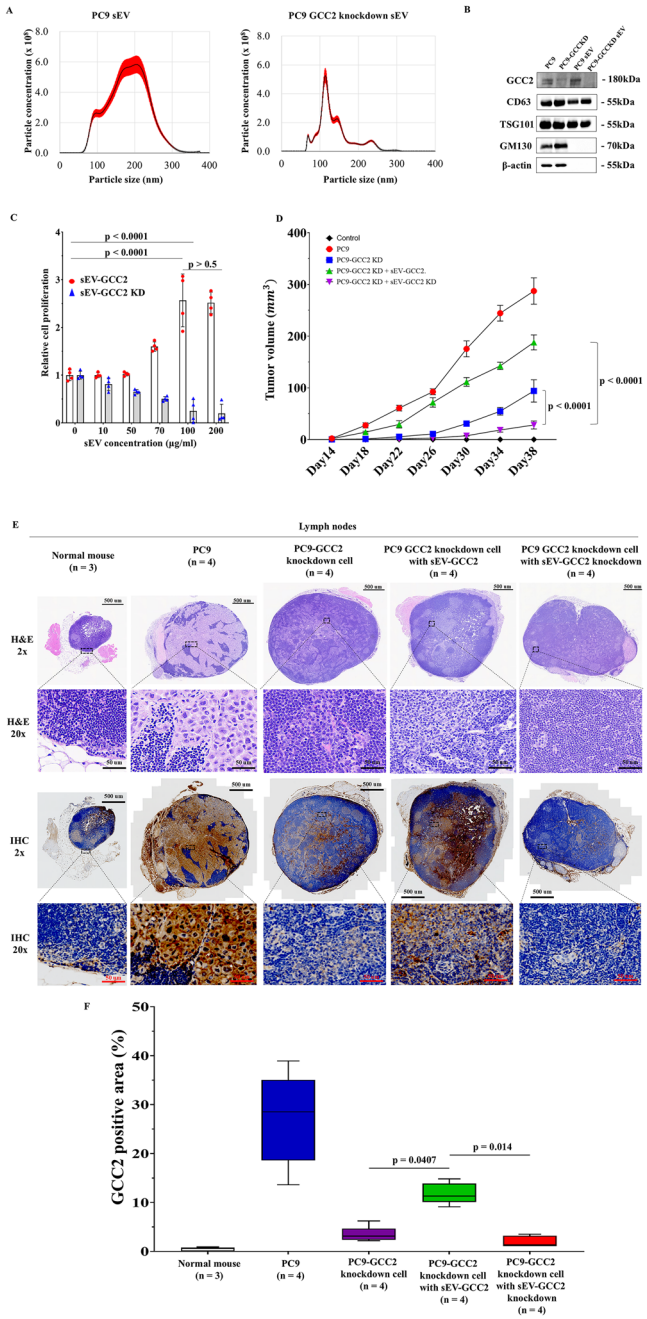

FIGURE 7 | Functional effects of sEV-GCC2 on cell proliferation, tumour growth and lymph node metastasis in lung adenocarcinoma models. (A) Nanoparticle tracking analysis (NTA) of sEVs derived from PC9 and GCC2-knockdown PC9 (PC9-GCC2 KD) cells. (B) Western blot analysis of GCC2, CD63, TSG101 and the Golgi marker GM130 in parental cells and their respective sEVs. (C) Cell proliferation of PC9-GCC2 KD cells treated with varying concentrations of sEVs from PC9 or PC9-GCC2 KD cells. (D) Tumour growth in vivo following subcutaneous footpad injection of PC9-GCC2 KD cells with phosphate-buffered saline (PBS), sEV-GCC2, or sEV-GCC2 KD. Data are shown as mean tumour volume ± SD. (E) Representative hematoxylin and eosin-stained and GCC2 immunohistochemistry images of lymph nodes from each mouse group, shown at low and high magnification. Scale bars are indicated. (F) Quantitative analysis of lymph node metastasis, including the percentage of GCC2-positive area within lymph nodes. Scale bars: 500 μm (2×) and 50 μm (20×). Data are presented as box plots; statistical significance was assessed by one-way ANOVA followed by Tukey's multiple comparisons test.

TABLE 3 | Simple and multiple cox-regression analysis for time to recurrence.

Variable	Simple cox regression						Multiple Cox regression					
	RR		OS		RFS		RR		OS		RFS	
	Hazard ratio (95% CI)	*P*-value	Hazard ratio (95% CI)	*P*-value	Hazard ratio (95% CI)	*P*-value	Hazard ratio (95% CI)	*P*-value	Hazard ratio (95% CI)	*P*-value	Hazard ratio (95% CI)	P-value
Age	1.524 (0.698–3.331)	0.290	1.656 (0.326–8.407)	0.543	1.615 (0.768–3.394)	0.206						
Sex	0.859 (0.398–1.853)	0.697	0.768 (0.154–3.823)	0.747	0.781 (0.377–1.618)	0.506						
Left lower lobe (tumour location)	2.761 (1.230–6.197)	0.014	5.181 (1.040–25.799)	0.045	2.763 (1.284–5.947)	0.009	2.370 (1.036–5.422)	0.041	5.181 (1.040–25.799)	0.045	2.426 (1.108–5.310)	0.027
Tumour size	1.635 (0.751–3.564)	0.216	1.271 (0.256–6.311)	0.769	1.484 (0.713–3.088)	0.291						
Pathological T stage	1.505 (0.696–3.257)	0.299	0.346 (0.040–2.967)	0.333	1.237 (0.590–2.593)	0.573						
Pathological N stage	8.335 (3.303–21.031)	< 0.001	0.047 ($5.3x10^{-11}$–$3.7x10^{7}$)	0.770	7.449 (2.990–18.556)	< 0.001	4.848 (1.799–13.067)	0.002			4.138 (1.536–11.152)	0.005
Pathological TNM stage	1.473 (0.680–3.188)	0.326	0.345 (0.040–2.953)	0.331	1.212 (0.578–2.540)	0.611						
Lymphatic invasion	4.051 (1.857–8.838)	< 0.001	1.373 (0.159–11.840)	0.773	3.985 (1.900–8.358)	< 0.001	2.970 (1.251–7.054)	0.014			3.343 (1.525–7.330)	0.003
Visceral pleural invasion	2.471 (1.134–5.384)	0.023	0.540 (0.063–4.639)	0.574	2.040 (0.963–4.323)	0.063	1.773 (0.782–4.020)	0.171				
Venous invasion	2.057 (0.708–5.977)	0.185	2.154 (0.250–18.538)	0.485	2.431 (0.926–6.378)	0.071						
sEV-GCC2	3.753 (1.717–8.200)	< 0.001	2.726 (0.497–14.958)	0.248	3.164 (1.489–6.724)	0.003	3.308 (1.465–7.467)	0.004			2.588 (1.181–5.675)	0.018

RR: Recurrence rate; OS: Overall survival; RFS: Recurrence-free survival.

tions, quantitative analyses demonstrated a significantly higher metastatic burden in the sEV-GCC2 group. Specifically, the proportion of mice with lymph node metastases and the extent of metastatic involvement per lymph node were higher than those in the GCC2-depleted sEV group (Table S4). Quantification of GCC2 immunoreactivity revealed a significantly greater GCC2-positive area in the lymph nodes of sEV-GCC2–treated mice ($P = 0.014$).

To further investigate whether GCC2 influences the molecular cargo of sEVs, sEVs derived from wild-type and GCC2-knockdown PC9 cells were subjected to small RNA sequencing. Unsupervised hierarchical clustering clearly separated samples by GCC2 status, indicating distinct miRNA expression profiles in sEVs (Figure S7A).

Differential expression analysis identified 58 upregulated and 89 downregulated miRNAs in sEVs from GCC2-knockdown cells compared to controls (Figure S7B), suggesting that GCC2 depletion is associated with substantial alterations in sEV miRNA cargo composition.

4 | Discussion

This multicentre study evaluated the diagnostic, prognostic and tumourigenic significance of sEV-GCC2 in early-stage lung ADC. Our findings show that sEV-GCC2 is elevated in patients with lung ADC and reflects tumour burden, correlating with clinical parameters, including pathological TNM stage, tumour location, pathological up-staging and survival outcomes (RR, OS and RFS).

Compared with our previous pilot study, the present work extends the clinical relevance of sEV-GCC2 beyond its diagnostic performance through multicentre validation, prognostic assessment and functional characterization.

Accurate risk stratification at the early stages is essential for improving survival and guiding the treatment of lung ADC (Bonanno et al. 2022; Rolfo et al. 2021). Liquid biopsy approaches using circulating tumour cells (CTCs), cell-free DNA (cfDNA) and sEVs offer non-invasive tools for diagnosis and monitoring(Alix-Panabières and Pantel 2021; W. Yu et al. 2021b). EV-based biomarkers are particularly attractive owing to their abundance, stability and ability to mirror tumour biology (Hessvik and Llorente 2018; Simpson et al. 2012). However, the diagnostic utility of EVs in early-stage lung cancer remains unclear.

sEVs encapsulate a wide spectrum of biomolecules reflective of their cellular origin, with more than 10,000 EV-associated proteins cataloged in databases, such as ExoCarta (Hessvik and Llorente 2018; Simpson et al. 2012). This proteomic diversity underlies their growing potential as cancer biomarkers, particularly in early-stage lung cancer, where conventional markers remain insufficient. In our study, sEV-GCC2 demonstrated strong diagnostic performance in age- and sex-adjusted analyses (AUC: 0.904) and effectively distinguished the earliest pathological stages (TisN0–T1miN0) from controls (AUC: 0.781) (Figures 2; Table S2). These findings suggest the utility of sEV-GCC2 as a sensitive marker for early detection of lung ADC. While imaging- and ctDNA-based assays remain standard approaches, sEV-GCC2 may provide complementary information, although direct comparisons are not feasible.

GCC2 is a Golgi-associated coiled-coil protein that is involved in Golgi maintenance and vesicular trafficking (Brown et al. 2011; Burguete et al. 2008; Hayes et al. 2009; Luke et al. 2003; Reddy et al. 2006; Sinka et al. 2008). It has also been implicated in tumourigenesis, including as a fusion partner in ALK-rearranged NSCLC (Jiang et al. 2018; Vendrell et al. 2017), although its roles in EV biology and as a liquid biomarker have not yet been fully elucidated. Given its established role in post-Golgi trafficking, GCC2 may be preferentially incorporated into sEVs through Golgi–endosomal transport pathways, thereby providing a plausible mechanistic basis for its enrichment in sEVs.

Our pilot study is the first to propose, in a small cohort of patients, sEV-GCC2 as a diagnostic marker in early-stage lung ADC ($n = 30$) (Jeong et al. 2021). The current study expands on this by using a larger multicentre cohort, including survival data, and performing functional validation, while focusing exclusively on lung ADC to reduce histological variability.

The sEV-GCC2 levels were independently associated with tumour location and pTNM stage. Interestingly, the concentrations were higher in tumours located in the left lower lobe (Table 2; Figure S1), although their clinical significance remains unclear.

Previous studies have suggested that tumours arising in the lower lobes may exhibit distinct clinical behaviours and prognostic implications, potentially related to anatomical factors such as lymphatic drainage patterns (Kudo et al. 2012; Ye et al. 2016). Accordingly, the association between the left lower lobe location and elevated sEV-GCC2 levels observed in this study should be interpreted as exploratory rather than indicative of a definitive location-specific biological effect.

In parallel, immunohistochemistry confirmed higher GCC2 expression in tumour tissues from advanced-stage cases, reinforcing the association between tumour burden and plasma sEV-GCC2 levels (Figure 4).

Preoperative sEV-GCC2 levels were also associated with pathological up-staging after surgery (AUC: 0.582; $P = 0.024$) (Figure 5, Table S3), suggesting a potential role in identifying occult pathological progression that is not evident during initial clinical staging. These findings may help guide postoperative decision-making, such as selecting an appropriate adjuvant therapy or intensifying surveillance in patients who are clinically understaged before surgery (Kirmani et al. 2013; Rocha et al. 2004; Riquet and Mordant 2013).

However, given the limited PPV observed in early-stage patients, the use of sEV-GCC2 as a stand-alone screening biomarker should be approached with caution. In this context, the specificity and clinical utility of sEV-GCC2 may be enhanced when integrated into a multimodal diagnostic framework alongside imaging findings or complementary biomarkers, such as circulating tumour DNA.

To assess the consistency of sEV isolation across institutions, standardized sEV protein yield and particle-normalized sEV protein content were compared among participating centers (Figure S8). No significant differences were observed, suggesting minimal batch effects across sites.

Regarding pathological upstaging, the discriminative performance of sEV-GCC2 was modest, and this finding should be interpreted as exploratory. Rather than serving as a determinant of clinical decision-making, sEV-GCC2 may function as an adjunctive risk stratification marker that supports clinical awareness of potential occult disease progression and may inform closer surveillance or more detailed pathological evaluation.

In survival analysis, elevated preoperative sEV-GCC2 ($\geq$ 73.88 pg/mL) predicted worse outcomes in RR, OS and RFS, even among patients with stage 0–IA1 (Figure 6). Despite the small number of events, sEV-GCC2 remained an independent prognostic factor in multivariate analysis. The lack of a statistically significant association with overall survival is likely attributable to the study cohort's early-stage composition and the limited number of deaths during follow-up. In this context, recurrence-related endpoints such as relapse-free survival and recurrence risk may more sensitively reflect the underlying tumour biology, whereas longer follow-up may be required to detect differences in overall survival.

The cut-off value for sEV-GCC2 (73.88 pg/mL) was determined using the Youden index within the study population. However, the cutoff values derived in this manner may be influenced by cohort composition and disease prevalence. Accordingly, the proposed threshold should be considered exploratory, and validation in independent, prospective cohorts is required before clinical application.

Functional studies have demonstrated that GCC2 plays a direct role in tumour progression. In vitro, GCC2 knockdown reduced cell migration (Figure S5), whereas in vivo administration of GCC2-containing sEVs enhanced tumour growth and lymph node metastasis (Figure 7). These findings support the notion that sEV-GCC2 is functionally involved in cancer progression beyond serving as a biomarker.

Quantitative analysis of lymph node metastasis further supported the conclusion that sEV-GCC2 promoted metastatic progression in vivo. Increased metastatic burden and a higher GCC2-positive area in lymph nodes from sEV-GCC2-treated mice indicate that sEV-associated GCC2 contributes to lymphatic dissemination, rather than representing a purely histological observation.

In line with these functional findings, comparative miRNA sequencing of sEVs derived from wild-type and GCC2-knockdown PC9 cells revealed distinct alterations in the sEV miRNA cargo composition (Figure S7), providing preliminary evidence that GCC2-dependent vesicle trafficking may influence the molecular content of secreted sEVs. These observations raise the possibility that sEV-associated GCC2 may represent a conceptual therapeutic target for modulating intercellular communication, although direct inhibition of GCC2 is likely limited by its essential role in Golgi integrity and vesicular trafficking.

Collectively, these data highlight the potential of sEV-GCC2 as a non-invasive biomarker with both diagnostic and prognostic utility for early-stage lung ADC. Its incorporation into clinical workflows may enhance perioperative decision-making and improve risk stratification.

Although this study provides compelling evidence supporting the diagnostic and prognostic value of sEV-GCC2 in early-stage lung adenocarcinoma, several limitations should be acknowledged. First, the analysis was restricted to lung adenocarcinoma and did not include other lung cancer subtypes or benign pulmonary diseases, thereby limiting the assessment of the biomarker specificity across broader disease contexts.

Second, healthy control samples were obtained from a single institution owing to the limited availability of well-characterized, low-dose CT-screened individuals without lung cancer, which may introduce selection bias and limit generalizability, despite standardized sample processing across centres. Finally, the retrospective design and the relatively short follow-up period, particularly in ultra-early-stage disease, constrain the comprehensive evaluation of clinical performance.

Accordingly, independent prospective studies that incorporate diverse disease controls and multicentre matched cohorts are required to confirm the clinical utility and specificity of sEV-GCC2. In conclusion, sEV-GCC2 is a novel and clinically relevant biomarker for early-stage lung ADC. This offers both mechanistic and translational value and may advance the implementation of EV-based liquid biopsy approaches in lung cancer management.

5 | Conclusions

This study identified sEV-GCC2 as a clinically relevant biomarker with diagnostic and prognostic value for early-stage lung adenocarcinoma. In addition to reflecting the tumour burden, sEV-GCC2 exhibited tumour-promoting activity in functional assays, underscoring its potential role not only as a liquid biopsy marker but also as a contributor to disease progression.

Authors Contributions

Byeong Hyeon Choi and Hyonggin An contributed equally to this work and are the first co-authors. Byeong Hyeon Choi, Hyonggin An, Yeonho Choi and Hyun Koo Kim designed the study and wrote the manuscript with input from all authors. Byeong Hyeon Choi, Hyonggin An: Investigation, Formal analysis, Methodology, Supervision, Validation, Visualization, Writing—original draft, writing—review and editing; Sukki Cho, Sungsoo Lee, Hyeong Ryul Kim, Jong Ho Cho, Jun Hee Lee, Ga Yoon Kim, Ok Hwa Jeon and Hyunku Shin: Conceptualization, Investigation, Resources, Supervision; Yeonho Choi and Hyun Koo Kim: Conceptualization, Investigation, Methodology, Validation, Visualization, Writing—review and editing and funding acquisition.

Acknowledgements

The authors have nothing to report.

Funding

This research was supported by a grant of the National Research Foundation of Korea (NRF) grant funded by the Korea government (MSIT) (grant number: RS-2025-00518091).

Ethics Statement

This multicentre retrospective clinical study was approved by the Institutional Review Board of Korea University Guro Hospital (2020GR0176) and all participating institutions (ClinicalTrials.gov identifier: NCT04529915). The study was conducted in accordance with the principles of the Declaration of Helsinki. This preclinical study was approved by the Institutional Animal Care and Use Committee of Korea University (KOREA-0216-0223-C1).

Conflicts of Interest

The authors declare that they have no competing interests.

Data Availability Statement

Data supporting the findings of this study are available from the corresponding author, Hyun Koo Kim, upon request.

Consent

Written informed consent was not required because the study was retrospective.

References

Adachi, H., K. Sakamaki, T. Nishii, et al. 2017. "Lobe-Specific Lymph Node Dissection as a Standard Procedure in Surgery For Non–Small Cell Lung Cancer: A Propensity Score Matching Study." *Journal of thoracic oncology* 12: 85–93.

Alix-Panabières, C., and K. Pantel. 2021. "Liquid Biopsy: From Discovery To Clinical Application." *Cancer discovery* 11: 858–873.

AmericanCancerSociety. 2018. *Global Cancer Facts & Figures 4th Edition*. American Cancer Society.

Bardelli, A., and K. Pantel. 2017. "Liquid Biopsies, What We Do Not Know (Yet)." *Cancer Cell* 31: 172–179.

Birim, Ö., A. P. Kappetein, T. Stijnen, and A. J. J. C. Bogers. 2005. "Meta-Analysis of Positron Emission Tomographic and Computed Tomographic Imaging in Detecting Mediastinal Lymph Node Metastases in Nonsmall Cell Lung Cancer." *Annals of Thoracic Surgery* 79: 375–382.

Bonanno, L., A. Dal Maso, A. Pavan, et al. 2022. "Liquid Biopsy and Non-Small Cell Lung Cancer: Are We Looking At The Tip Of The Iceberg?" *British Journal of Cancer* 127: 383–393.

Bossuyt, P. M., J. B. Reitsma, D. E. Bruns, et al. 2015. "STARD 2015: An Updated List Of Essential Items for Reporting Diagnostic Accuracy Studies." *Radiology* 277: 826–832.

Bott, M. J., A. P. Patel, T. D. Crabtree, et al. 2015. "Pathologic Upstaging in Patients Undergoing Resection for Stage I Non-Small Cell Lung Cancer: Are There Modifiable Predictors?" *Annals Of Thoracic Surgery* 100: 2048–2053.

Brown, F. C., C. H. Schindelhaim, and S. R. Pfeffer. 2011. "GCC185 Plays Independent Roles in Golgi Structure Maintenance and AP-1–Mediated Vesicle Tethering." *Journal of Cell Biology* 194: 779–787.

Burguete, A. S., T. D. Fenn, A. T. Brunger, and S. R. Pfeffer. 2008. "Rab and Arl GTPase Family Members Cooperate in the Localization Of the Golgin Gcc185." *Cell* 132: 286–298.

Goldstraw, P., K. Chansky, J. Crowley, et al. 2016. "The IASLC Lung Cancer Staging Project: Proposals for Revision of the TNM Stage Groupings in the Forthcoming (Eighth) Edition of the TNM Classification for Lung Cancer." *Journal of Thoracic Oncology* 11: 39–51.

Hayes, G. L., F. C. Brown, A. K. Haas, R. M. Nottingham, F. A. Barr, and S. R. Pfeffer. 2009. "Multiple Rab GTPase Binding Sites in GCC185 Suggest a Model for Vesicle Tethering at the Trans-Golgi." *Molecular Biology of the Cell* 20: 209–217.

Hessvik, N. P., and A. Llorente. 2018. "Current Knowledge on Exosome Biogenesis and Release." *Cellular and Molecular Life Sciences* 75: 193–208.

Hoseok, I., and J. Y. Cho. 2015. "Lung Cancer Biomarkers." *Advances in Clinical Chemistry* 72: 107–170.

Jayaseelan, V. P. 2020. "Emerging Role of Exosomes as Promising Diagnostic Tool for Cancer." *Cancer Gene Therapy* 27: 395–398.

Jeltema, D., K. Abbott, and N. Yan. 2023. "STING Trafficking as a New Dimension of Immune Signaling." *Journal of Experimental Medicine* 220: e20220990.

Jeong, H., B. H. Choi, J. Park, et al. 2021. "GCC2 as a New Early Diagnostic Biomarker for Non-Small Cell Lung Cancer." *Cancers* 13: 5482.

Jiang, J., X. Wu, X. Tong, et al. 2018. "GCC2-ALK as a Targetable Fusion in Lung Adenocarcinoma and Its Enduring Clinical Responses to ALK Inhibitors." *Lung Cancer* 115: 5–11.

Kilkenny, C., W. J. Browne, I. C. Cuthill, M. Emerson, and D. G. Altman. 2012. "Improving Bioscience Research Reporting: the ARRIVE Guidelines for Reporting Animal Research." *Osteoarthritis and Cartilage* 20: 256–260.

Kirmani, B. H., R. C. Rintoul, T. Win, et al. 2013. "Stage Migration: Results Of Lymph Node Dissection in the Era of Modern Imaging and Invasive Staging for Lung Cancer." *European Journal of Cardio-Thoracic Surgery* 43: 104–110.

Kudo, Y., H. Saji, Y. Shimada, et al. 2012. "Do Tumours Located in the Left Lower Lobe Have Worse Outcomes in Lymph Node-Positive Non-Small Cell Lung Cancer Than Tumours in Other Lobes?" *European Journal Of Cardio-Thoracic Surgery* 42: 414–419.

Luke, M. R., L. Kjer-Nielsen, D. L. Brown, J. L. Stow, and P. A. Gleeson. 2003. "GRIP Domain-Mediated Targeting of Two New Coiled-Coil Proteins, GCC88 and GCC185, to Subcompartments of the Trans-Golgi Network." *Journal of Biological Chemistry* 278: 4216–4226.

Mazzone, P. J., G. A. Silvestri, S. Patel, et al. 2018. "Screening for Lung Cancer: Chest Guideline and Expert Panel Report." *Chest* 153: 954–985.

Mazzone, P. J., G. A. Silvestri, L. H. Souter, et al. 2021. "Screening for Lung Cancer: CHEST Guideline and Expert Panel Report." *Chest* 160: e427–e494.

Mulshine, J. L., and D. C. Sullivan. 2005. "Lung Cancer Screening." *New England Journal of Medicine* 352: 2714–2720.

Palmirotta, R., D. Lovero, P. Cafforio, et al. 2018. "Liquid Biopsy of Cancer: A Multimodal Diagnostic Tool in Clinical Oncology." *Therapeutic Advances in Medical Oncology* 10: 1758835918794630.

Pantel, K., and C. Alix-Panabières. 2019. "Liquid Biopsy and Minimal Residual Disease—Latest Advances and Implications for Cure." *Nature Reviews Clinical Oncology* 16: 409–424.

Reck, M., and K. F. Rabe. 2017. "Precision Diagnosis and Treatment for Advanced Non–Small-Cell Lung Cancer." *New England Journal of Medicine* 377: 849–861.

Reddy, J. V., A. S. Burguete, K. Sridevi, I. G. Ganley, R. M. Nottingham, and S. R. Pfeffer. 2006. "A Functional Role for the GCC185 Golgin in Mannose 6-Phosphate Receptor Recycling." *Molecular biology of the cell* 17: 4353–4363.

Riquet, M., and P. Mordant. 2013. "Incomplete Intrapulmonary Lymph Node Retrieval After Routine Pathologic Examination of Resected Lung Cancer." *Translational Lung Cancer Research* 2, no. 1: 1–2.

Robinson, E. M., I. K. Ilonen, K. S. Tan, et al. 2020. "Prevalence of Occult Peribronchial N1 Nodal Metastasis in Peripheral Clinical N0 Small (≤ 2

cm) Non-Small Cell Lung Cancer." *Annals of Thoracic Surgery* 109: 270–276.

Rocha, A. T., M. Mccormack, G. Montana, and G. Schreiber. 2004. "Association Between Lower Lobe Location and Upstaging for Early-Stage Non-Small Cell Lung Cancer." *Chest* 125: 1424–1430.

Rolfo, C., P. Mack, G. V. Scagliotti, et al. 2021. "Liquid Biopsy for Advanced NSCLC: A Consensus Statement From the International Association for the Study of Lung Cancer." *Journal of Thoracic Oncology* 16: 1647–1662.

Rolfo, C., P. C. Mack, G. V. Scagliotti, et al. 2018. "Liquid Biopsy for Advanced Non-Small Cell Lung Cancer (NSCLC): A Statement Paper From the IASLC." *Journal of Thoracic Oncology* 13: 1248–1268.

Russell, P. A., Z. Wainer, G. M. Wright, et al. 2011. "Does Lung Adenocarcinoma Subtype Predict Patient Survival?: A Clinicopathologic Study Based On The New International Association for the Study of Lung Cancer/American Thoracic Society/European Respiratory Society International Multidisciplinary Lung Adenocarcinoma Classification." *Journal of Thoracic Oncology* 6: 1496–1504.

Sauerbrei, W., S. E. Taube, L. M. Mcshane, M. M. Cavenagh, and D. G. Altman. 2018. "Reporting Recommendations for Tumor Marker Prognostic Studies (REMARK): An Abridged Explanation and Elaboration." *JNCI: Journal of the National Cancer Institute* 110: 803–811.

Siegel, R. L., T. B. Kratzer, A. N. Giaquinto, H. Sung, and A. Jemal. 2025. "Cancer statistics, 2025." *CA: A Cancer Journal for Clinicians* 75, no. 1: 10–45. Portico. https://doi.org/10.3322/caac.21871.

Simpson, R. J., H. Kalra, and S. Mathivanan. 2012. "eExoCarta as a Resource for Exosomal Research." *Journal of Extracellular Vesicles* 1: 18374.

Sinka, R., A. K. Gillingham, V. Kondylis, and S. Munro. 2008. "Golgi Coiled-Coil Proteins Contain Multiple Binding Sites for Rab Family G Proteins." *Journal of Cell Biology* 183: 607–615.

Travis, W. D., E. Brambilla, A. G. Nicholson, et al. 2015. "The 2015 World Health Organization Classification of Lung Tumors: Impact of Genetic, Clinical and Radiologic Advances Since the 2004 Classification." *Journal of Thoracic Oncology* 10: 1243–1260.

Tu, X., T. T. Chu, D. Jeltema, et al. 2022. "Interruption of Post-Golgi STING Trafficking Activates Tonic Interferon Signaling." *Nature Communications* 13: 6977.

Vendrell, J. A., S. Taviaux, B. Béganton, et al. 2017. "Detection of Known and Novel ALK Fusion Transcripts in Lung Cancer Patients Using Next-Generation Sequencing Approaches." *Scientific Reports* 7: 12510.

Xu, R., A. Rai, M. Chen, W. Suwakulsiri, D. W. Greening, and R. J. Simpson. 2018. "Extracellular Vesicles in Cancer—Implications for Future Improvements in Cancer Care." *Nature Reviews Clinical Oncology* 15: 617–638.

Ye, W. F., X. Xie, H. Yang, et al. 2016. "Resectable Left Lower Lobe Non–Small Cell Lung Cancer With Lymph Node Metastasis is Related to Unfavorable Outcomes." *Chinese Journal of Cancer* 35: 7.

Yu, F., M. Liang, W. Wu, et al. 2021a. "Upregulation of Long Non-Coding RNA GCC2-AS1 Facilitates Malignant Phenotypes and Correlated With Unfavorable Prognosis for Lung Adenocarcinoma." *Frontiers in oncology* 10: 628608.

Yu, W., J. Hurley, D. Roberts, et al. 2021b. "Exosome-Based Liquid Biopsies in Cancer: Opportunities and Challenges." *Annals of Oncology* 32: 466–477.

Supporting Information

Additional supporting information can be found online in the Supporting Information section.

Supporting Information: Supplemental File 1_STARD-2015-Checklist.docx **Supporting Information**: Supplemental File 2_REMARK-Checklist.docx **Supporting Information**: Supplemental File 3_ARRIVE Checklist—E10 only.pdf **Supplementary Figure 1**: sEV-GCC2 concentrations in the lung lobes of patients with lung adenocarcinoma. **Supplement Figure 2**: Kaplan–Meier analysis of time to recurrence, overall survival, and recurrence-free survival in patients with stage IA3 disease. **Supplementary Figure 3**: Kaplan–Meier analysis of time to overall survival and recurrence-free survival in patients with stage IB disease **Supplementary Figure 4**: Kaplan–Meier analysis of time to recurrence, overall survival, and recurrence-free survival in patients with stage IIB disease **Supplementary Figure 5**: GCC2 knockdown reduces migration in lung adenocarcinoma cells in vitro. **Supplementary Figure 6**: Effects of GCC2 depletion on ESCRT-related proteins involved in sEV biogenesis. **Supplementary Figure 7**: miRNA cargo profiling of sEVs derived from wild-type and GCC2-knockdown PC9 lung adenocarcinoma cells. **Supplementary Figure 8**: Assessment of sEV protein yield and particle-normalized protein consistency across participating institutions. **Supplementary Table 1**: Research flow chart. **Supplementary Table 2**: Age- and sex-adjusted ROC curve analysis of the concentration of sEV-GCC2, sEV and size of sEV **Supplementary Table 3**: Characteristics of pathological-up migration. **Supplementary Table 4**: Histological finding of mice lymph nodes.